Simple Adjoint Methods for Single-Doppler Wind Analysis with a Strong Constraint of Mass Conservation

QIN XU AND CHONG-JIAN QIU*

Cooperative Institute for Mesoscale Meteorological Studies, University of Oklahoma/NOAA, Norman, Oklahoma

(Manuscript received 12 February 1993, in final form 8 July 1993)

ABSTRACT

Three schemes are developed to incorporate a strong constraint of (incompressible) mass conservation into the basic scheme (scheme B) of the simple adjoint method of Qiu and Xu for retrieving the time-mean wind field from a sequence of single-Doppler scans. In the first scheme (S1), the two-dimensional wind field on a surface normal to the radar beam is partitioned into an irrotational component expressed by the velocity potential and a nondivergent component expressed by the streamfunction. The velocity potential can be obtained directly from single-Doppler observations, and the streamfunction is retrieved by the adjoint method. In this way, the retrieved wind field satisfies the mass conservation equation precisely. The second scheme (S2) is the same as scheme S1 except that a spectral expression is used to replace the grid representation of the streamfunction. The third scheme (S3) imposes a strong mass conservation constraint through a postadjustment after the wind field is retrieved by scheme B with a weak mass conservation constraint. These schemes are tested with artificial data. Their relative merits and disadvantages are examined and compared in terms of accuracy, convergence rate, sensitivity to errors, and computational efficiency.

1. Introduction

A simple adjoint method was recently developed by Qiu and Xu (1992, henceforth referred to as QX92) for retrieving the time-mean (or running mean) wind field from a sequence of single-Doppler scans. The method assumes Lagrangian conservation of reflectivity. Previous methods based on the same advection equation have to deal with the problems of nonuniqueness and/or singularity. These two problems are eliminated by using a sequence of observations. The method was tested with artificial data in QX92 and also modified and tested with the Phoenix II field experiment data (Xu et al. 1994a,b). The results showed that using data over a sequence of time levels to retrieve the time-mean winds not only increased the accuracy of retrieval but also made the method less sensitive to data errors and temporal wind fluctuations. It was also found that incorporating the (incompressible) mass conservation equation into the method, even as a weak constraint (called scheme W), could significantly increase the accuracy of the retrieved winds. However, since the mass conservation equation was used only as a weak constraint, the retrieved wind field was not ensured to satisfy the mass conservation equation very accurately. For some applications, it is desirable that the retrieved wind field satisfies the mass conservation equation accurately, especially when the retrieved wind field is used to initialize a numerical model (otherwise, spurious waves may be generated). In this paper, three schemes (S1, S2, and S3) are developed and tested with artificial data for incorporating a strong mass conservation constraint into the basic scheme of QX92 (called scheme B, without a mass conservation constraint). In scheme S1, the two-dimensional wind field on a surface normal to the radar beam is partitioned into an irrotational component and a nondivergent component, expressed by the velocity potential and streamfunction, respectively. Since the velocity potential can be obtained directly from single-Doppler observations and only the streamfunction is retrieved by the adjoint method, the retrieved total wind field satisfies the mass conservation equation precisely. Scheme S2 is the same as scheme S1 except that a spectral expression is used to replace the grid representation of the streamfunction. Scheme S3 imposes the strong mass conservation constraint through a postadjustment, after the wind field is retrieved by scheme W. Scheme S1 and scheme S2 are described in the next section. The experiment results with artificial data are presented in section 3 where comparisons are also made with the previous schemes (B and W) of QX92. Scheme S3 is proposed and tested in section 4. Conclusions follow in section 5.

* Current affiliation: Department of Atmospheric Science, Lanzhou University, Lanzhou, People's Republic of China.

Corresponding author address: Dr. Qin Xu, CIMMS, University of Oklahoma/NOAA, Room 1110, 100 E. Boyd, Norman, OK 73019-0628.

2. Description of scheme S1 and scheme S2

a. Formulation with a strong constraint of mass conservation

For simplicity, we consider the following incompressible Boussinesq mass conservation equation in a fixed cross section, say, $x = x_1$ normal to the Doppler radar beam:

$$\partial_y v + \partial_z w = -\partial_x u = -\partial_x u_{ob} \equiv D_{ob}(x_1, y, z, t), \tag{2.1}$$

where (u, v, w) is the velocity vector and $u = u_{ob}$ is measured by the Doppler radar. [For a real-data application, a spherical coordinate system should be used with u representing the observed radial-component wind and (v, w) being the unobserved two-dimensional wind vector on the spherical surface of a fixed radial distance from the radar.] The two-dimensional wind vector (v, w) can be partitioned as follows:

$$v = \partial_y \varphi - \partial_z \psi, \quad w = \partial_z \varphi + \partial_y \psi, \tag{2.2}$$

where φ is the velocity potential for the irrotational part of (v, w) and ψ is the streamfunction for the nondivergent part of (v, w). The velocity potential φ can be determined by the following equation and boundary condition:

$$\partial_y^2 \varphi + \partial_z^2 \varphi = D_{ob} \tag{2.3a}$$

for $x = x_1$ and $(y, z) \in \Omega$,

$$\varphi = 0 \tag{2.3b}$$

at the boundary of Ω, where Ω is a fixed data-covered (for the retrieving period) region in the cross section $x = x_1$. Here, (2.3a) is obtained by substituting (2.2) into (2.1). Because the homogeneous boundary condition is used for φ in (2.3b), the harmonic part should be included in the nondivergent part and, thus, ψ should satisfy the Laplace equation with nonhomogeneous boundary condition [Lynch (1989); also see sections 2.7 and 2.10 of Batchelor (1967)]. If the streamfunction ψ can be retrieved, then the three-dimensional wind (u_{ob}, v, w) will exactly satisfy the mass conservation constraint (2.1). The adjoint method for retrieving ψ is derived as follows.

As in QX92, the model's equation is the Lagrangian conservation of nondimensional reflectivity η:

$$\partial_t \eta + u\partial_x \eta + v\partial_y \eta + w\partial_z \eta = 0. \tag{2.4}$$

The objective is to find the best time-mean estimate (averaged over a period τ) of the velocity field (v, w) that gives the best "prediction" η_e of the reflectivity field in terms of minimizing the following cost function

$$J = \int_0^\tau \iint_\Omega D dy dz dt \quad \text{with} \quad D \equiv P(t)(\eta_e - \eta_{ob})^2, \tag{2.5}$$

where $P(t)$ is a nondimensional weight and η_{ob} is the observation of η. Here, η_e is the reflectivity "predicted" from the following equation and conditions

$$\partial_t \eta_e - (\partial_z \psi_e)(\partial_y \eta_e) + (\partial_y \psi_e)(\partial_z \eta_e) = A_{ob} \tag{2.6}$$

for $0 < t < \tau$, $x = x_1$, and $(y, z) \in \Omega$,

$$\eta_e(t, y, z) = \eta_{ob}(t, x_1, y, z) \tag{2.7}$$

at the upstream boundary of Ω,

$$\eta_e(0, y, z) = \eta_{ob}(0, x_1, y, z), \tag{2.8}$$

where ψ_e is a time-mean estimate of ψ and $A_{ob} \equiv -u_{ob}(\partial_x \eta_{ob}) - (\partial_y \varphi)(\partial_y \eta_{ob}) - (\partial_z \varphi)(\partial_z \eta_{ob})$ can be obtained from the observation as φ is solved from (2.3a) and (2.3b). Here, by "upstream boundary" we mean those segments of the domain boundary where the wind vectors are inward. Since $x = x_1$ is fixed, η_e can be considered as a function of (t, y, z) only and ψ_e a function of (y, z) only.

b. Scheme S1

We denote by $\delta\psi$ the variation of ψ_e, and by $(\delta\eta, \delta J)$ the resulted variations of (η, J). The leading-order variations of (2.6)–(2.8) are

$$\partial_t \delta\eta - (\partial_z \psi_e)(\partial_y \delta\eta) + (\partial_y \psi_e)(\partial_z \delta\eta) = (\partial_z \delta\psi)(\partial_y \eta_e) - (\partial_y \delta\psi)(\partial_z \eta_e) \tag{2.9}$$

for $0 < t < \tau$, $x = x_1$, and $(y, z) \in \Omega$,

$$\delta\eta(t, y, z) = 0 \tag{2.10}$$

at the upstream boundary of Ω,

$$\delta\eta(0, y, z) = 0. \tag{2.11}$$

The associated adjoint formulation for η^* is given as follows:

$$-\partial_t \eta^* + \partial_y(\eta^* \partial_z \psi_e) - \partial_z(\eta^* \partial_y \psi_e) = -\partial_\eta D \equiv -2P(t)(\eta_e - \eta_{ob}) \tag{2.12}$$

for $0 < t < \tau$, $x = x_1$, and $(y, z) \in \Omega$,

$$\eta^*(t, y, z) = 0 \tag{2.13}$$

at the downstream boundary of Ω,

$$\eta^*(\tau, y, z) = 0. \tag{2.14}$$

By using integration by parts, we obtain from $\int_0^\tau \iint_\Omega \{\eta^* [\text{Eq. (2.9)}] - [\text{Eq. (2.12)}]\delta\eta\} dy dz dt$:

$$\iint_\Omega \left\{ \int_0^\tau [\partial_z(\eta^* \partial_y \eta_e) - \partial_y(\eta^* \partial_z \eta_e)] dt \right\} \delta\psi dy dz = \delta J.$$

This, as explained in QX92, implies that the gradient of the cost function J with respect to ψ (at each grid point) has the following explicit expression:

$$\nabla_\psi J = \int [\partial_z(\eta^* \partial_y \eta_e) - \partial_y(\eta^* \partial_z \eta_e)]dt. \quad (2.15)$$

The gradient in (2.15) gives the direction of the steepest descent of J at ψ_e. Along this direction, one can find the next guess for ψ_e. The iteration is performed as follows:

(i) Give the initial guess $\psi_e = \psi_0 = 0$ and integrate (2.6)–(2.8) forward in time, from 0 to τ, and store the computed η_e field.

(ii) Integrate the adjoint equations (2.12)–(2.14) backward in time, from τ to 0, and compute the gradient of J in (2.15) with respect to $\psi_e = \psi_0$ (at every grid point).

(iii) Use the conjugate-gradient subroutine to find the new guess $\psi_e = \psi_1$ and go back to (i). The general mathematic theory of the adjoint method can be found in Cacuci (1981) and Talagrand and Courtier (1987). The standard leapfrog scheme, with the Euler scheme for the initial time step (Haltiner and Williams 1979), is used to integrate the control equation and adjoint equation. The numerical code is designed carefully to ensure the conjugate property between the discretized operator and adjoint operator. The detailed process of finding the discrete adjoint from a discrete model can be found in Thacker and Long (1988).

c. Scheme S2

This scheme is the same as scheme S1, except that ψ_e is expressed by the following truncated spectral expansion:

$$\psi_e = \sum\sum \left[A_{n,k} \cos\left(\frac{n\pi y}{L_1}\right)\cos\left(\frac{k\pi z}{L_2}\right) + B_{n,k} \sin\left(\frac{n\pi y}{L_1}\right)\cos\left(\frac{k\pi z}{L_2}\right) + C_{n,k} \cos\left(\frac{n\pi y}{L_1}\right)\sin\left(\frac{k\pi z}{L_2}\right) + D_{n,k} \sin\left(\frac{n\pi y}{L_1}\right)\sin\left(\frac{k\pi z}{L_2}\right)\right], \quad (2.16)$$

where the double summations are for n (from 1 to 9) and k (from 1 to 9), $L_1 = L_2 = 2L$, $L \times L = \Omega$ is as in (2.3), and $A_{n,k}$, $B_{n,k}$, $C_{n,k}$ and $D_{n,k}$ are unknown spectral coefficients and need to be retrieved. Because ψ is not generally periodic in Ω, long-wave components ($n = 1$, $k = 1$) are included in (2.16).

The gradient of the cost function J with respect to the spectral coefficients can be derived by using the same adjoint method that leads to (2.15), except that the variation $\delta\psi$ in (2.9) is made to the spectral coefficients of ψ_e. The gradient components have the following explicit expression

$$\begin{aligned}
\frac{\partial J}{\partial A_{n,k}} &= \int\int_\Omega \left[\left(\frac{k\pi}{L_2}\right)\left(\int_0^\tau \eta^* \partial_y \eta_e dt\right)\cos\left(\frac{n\pi y}{L_1}\right)\sin\left(\frac{k\pi z}{L_2}\right) - \left(\frac{n\pi}{L_1}\right)\left(\int_0^\tau \eta^* \partial_z \eta_e dt\right)\sin\left(\frac{n\pi y}{L_1}\right)\cos\left(\frac{k\pi z}{L_2}\right)\right] d\Omega,\\
\frac{\partial J}{\partial B_{n,k}} &= \int\int_\Omega \left[\left(\frac{k\pi}{L_2}\right)\left(\int_0^\tau \eta^* \partial_y \eta_e dt\right)\sin\left(\frac{n\pi y}{L_1}\right)\sin\left(\frac{k\pi z}{L_2}\right) + \left(\frac{n\pi}{L_1}\right)\left(\int_0^\tau \eta^* \partial_z \eta_e dt\right)\cos\left(\frac{n\pi y}{L_1}\right)\cos\left(\frac{k\pi z}{L_2}\right)\right] d\Omega,\\
\frac{\partial J}{\partial C_{n,k}} &= -\int\int_\Omega \left[\left(\frac{k\pi}{L_2}\right)\left(\int_0^\tau \eta^* \partial_y \eta_e dt\right)\cos\left(\frac{n\pi y}{L_1}\right)\cos\left(\frac{k\pi z}{L_2}\right) + \left(\frac{n\pi}{L_1}\right)\left(\int_0^\tau \eta^* \partial_z \eta_e dt\right)\sin\left(\frac{n\pi y}{L_1}\right)\sin\left(\frac{k\pi z}{L_2}\right)\right] d\Omega,\\
\frac{\partial J}{\partial D_{n,k}} &= -\int\int_\Omega \left[\left(\frac{k\pi}{L_2}\right)\left(\int_0^\tau \eta^* \partial_y \eta_e dt\right)\sin\left(\frac{n\pi y}{L_1}\right)\cos\left(\frac{k\pi z}{L_2}\right) - \left(\frac{n\pi}{L_1}\right)\left(\int_0^\tau \eta^* \partial_z \eta_e dt\right)\cos\left(\frac{n\pi y}{L_1}\right)\sin\left(\frac{k\pi z}{L_2}\right)\right] d\Omega,
\end{aligned} \quad (2.17)$$

Here, η^* satisfies the adjoint problem in (2.12)–(2.14). The gradient in (2.17) gives the direction of the steepest descent of J with respect to the spectral coefficients of ψ_e. The iteration is performed through the same steps (i)–(iii) as in scheme S1, except that the gradient of J is computed from (2.17), while $\partial_z\psi_e$ and $\partial_y\psi_e$ in (2.6) and (2.12) are computed directly from the retrieved spectral coefficients without using finite differences.

3. Experiments and comparisons between schemes B, W, S1, and S2

Numerical experiments are conducted and compared for the following four schemes:

(i) scheme B without a mass conservation constraint [see (2.13) of QX92],

(ii) scheme W with a weak mass conservation constraint [see (2.16) of QX92],

(iii) scheme S1 with a strong mass conservation constraint and grid representation of ψ_e, and

(iv) scheme S2 with a strong mass conservation constraint and spectral representation of ψ_e.

All the experiments use artificial data generated by integrating (2.6)–(2.8). Note that the velocity potential φ can be computed directly from (2.3) with the observed radial-component wind divergence D_{ob} and this computation is independent of the adjoint method for retrieving the time-mean streamfunction. Thus, for the purpose of testing the adjoint method and without loss of generality, artificial data can be generated simply with $\varphi = 0$, $D_{ob} = 0$ in (2.3) and $A_{ob} = 0$ in (2.6). Two types of artificial data are generated: (i) error-free data, and (ii) error-contaminated data (with 25% observational error, 25% equation error, and 25% wind fluctuation). To generate the error-free data, we freely specify (by using filtered random functions as in QX92) the "true" time-mean streamfunction and "true" reflectivity field at the initial time and at the domain boundaries (Fig. 1). The error-free reflectivity data within the domain for the later time, $0 < t \leq \tau$, are generated by integrating the control equation (2.6)–(2.8). The error-contaminated reflectivity data are generated with the following modifications. First, random temporal fluctuations (25% relative to the time-mean wind) are included in the wind field to simulate the real wind fluctuation. Then, a random source term (25% relative to the advection term) is added to the right-hand side of (2.6) to simulate the equation error when (2.6) is used to generate the reflectivity field. After this, a random "observational" error (25% relative) is added to the above generated reflectivity field.

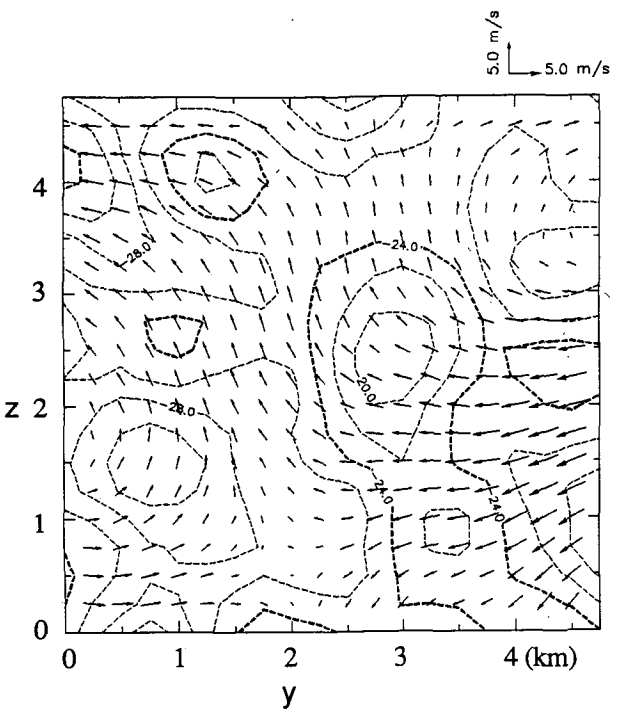

FIG. 1. "True" mean wind field and initial reflectivity field in the y–z cross section (normal to the radar beam).

In all the experiments, the initial guesses of winds are chosen to be zero and the finite-difference method is used to integrate the control equation and adjoint equation. The computational domain is covered by 20 × 20 meshes with the resolution $\Delta y = \Delta z = 250$ m. The time step is $\Delta t = 10$ s. It is assumed that the observational data are available at every grid point and every six time steps, that is, every $\Delta\tau = 6\Delta t = 60$ s. For simplicity, $P(t) = 1$ is used for all the schemes and the weight q for the weak mass conservation constraint in scheme W [see (2.15) of QX92] is specified as $q = k\sigma_\eta^2$ with $k = 500\ \text{s}^2$. Here, σ_η is the root mean square of the time–spatial variation of η. The accuracy of the retrieved wind can be measured by the relative rms error (RRE):

$$\text{RRE} = \frac{\|(\Delta u, \Delta v)\|}{\|(v_m, w_m)\|},$$

where $\|(a, b)\|^2 \equiv \Omega^{-1} \int\int_\Omega (a^2 + b^2) dydz$, $(\Delta u, \Delta v) \equiv (v_e - v_m, w_e - w_m)$, $(\ )_m \equiv \tau^{-1} \int_0^\tau (\ ) dt$, and (v_m, w_m) is the time-mean of the "true" wind. With RRE as a measure of accuracy for the retrieved time-mean wind field, the convergence rate, sensitivity to errors, and computational efficiency are examined in the following subsections.

a. Convergence rate

The experiments in this subsection use the error-free artificial data (first type). Figures 2a,b show how the RREs change with the number of iterations in the four experiments. The experiments in Fig. 2a use only three time levels of observation (i.e., $N \equiv \tau/\Delta\tau = 2$ time intervals). The experiments in Fig. 2b use six time levels of observation ($N = 5$ time intervals) and the results are significantly improved for all the schemes, which is consistent with the basic result in QX92. Clearly, scheme S2 converges most rapidly, while scheme S1 converges most slowly. Note that for scheme S1 the RRE undergoes an increase during the initial steps of iteration, although the cost function J decreases continuously (not shown). Scheme W converges slightly slower than scheme S2 but gives the most accurate retrieval. The limited accuracy for scheme S2 is partially related to the limited resolution of the truncated spectral representation of ψ_e in (2.16). By in-

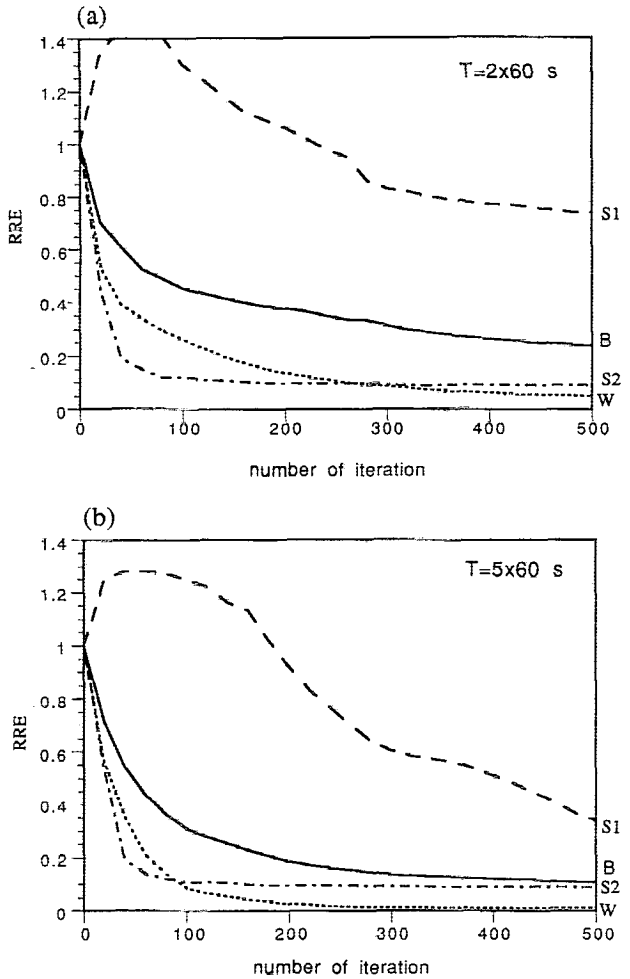

FIG. 2. RRE versus number of iteration for experiments with error-free data. (a) $N = 2$, (b) $N = 5$, where $N \equiv \tau/\Delta\tau$ is the number of time intervals covered by the retrieving time τ. The four curves (labeled with B, W, S1, and S2 on the right side) correspond to the four schemes.

cluding more spectral components in (2.16), scheme S2 can produce more accurate retrieval but still hardly as accurate as the retrieval of scheme W (with error-free data).

When the number of iterations is not limited and the iteration is continued until the RRE reaches the minimum (and the cost function J reaches zero or nearly zero since the data are error-free), an "optimal" retrieval is obtained for each scheme. The results are shown in Table 1. When $N = 2$, scheme W gives the best "optimal" retrieval and scheme S2 gives the second best "optimal" retrieval. When $N = 5$, both scheme W and scheme S1 give the best "optimal" retrieval, but scheme S1 requests much longer iteration. Scheme S2 gives the worst "optimal" retrieval due to the limited resolution of (2.16).

As shown in Table 1, although the data are error-free (and the cost function J reaches zero or nearly zero), the "optimal" retrieval errors are not very close to zero except for scheme W and scheme S1 with $N = 5$. When $N = 2$, the data do not seem to contain enough information to accurately determine the wind fields and, as explained in QX92, this can occur for all schemes (or scheme B) if the reflectivity gradient remains nearly zero (or the winds remain nearly parallel to the reflectivity contours) in a local region of the cross section during the retrieving time period. This explains why the retrieval errors are relatively large or not very close to zero for all the four schemes with $N = 2$. The situation seems somewhat similar to the "ill-posedness" demonstrated by Kapitza (1991) for the temperature retrieval from simulated error-free single-Doppler data with a full adjoint model. When more data ($N = 5$) are used and the mass conservation constraint is introduced, the retrieval errors reduce to nearly zero (0.3%) for scheme W and scheme S1. Scheme B does not use the mass conservation constraint, so the retrieval error (3.2%) is not very close to zero even for $N = 5$. Scheme S2 uses truncated spectral expression, so the retrieval error (8.4%) cannot be very small even for $N = 5$.

b. Sensitivity to errors

The experiments in this subsection use the error-contaminated artificial data (with 25% observational error, 25% equation error, and 25% wind fluctuation). The RREs versus the number of iteration are shown in Fig. 3a for $N = 2$ and Fig. 3b for $N = 5$. The results in Fig. 3b are significantly better than in Fig. 3a for all the schemes and this is, again, consistent with the result of QX92. Scheme S2 converges most rapidly, while scheme S1 converges most slowly. As in Figs. 2a,b, here the RRE for scheme S1 also undergoes an increase during the initial steps of iteration, although the cost function J decreases continuously (not shown). Since the data and equation are not error-free, there is an optimal number of iteration that gives the minimum RRE. The data and equation errors are responsible for

TABLE 1. RRE for "optimal" retrieval with error-free data.

$\tau = N\Delta\tau$	Scheme	RRE (%)	Number of iterations
120 s	B	16.5	1140
	W	1.7	1020
	S1	16.2	2200
	S2	9.0	460
300 s	B	3.2	1500
	W	0.3	820
	S1	0.3	3000
	S2	8.4	660

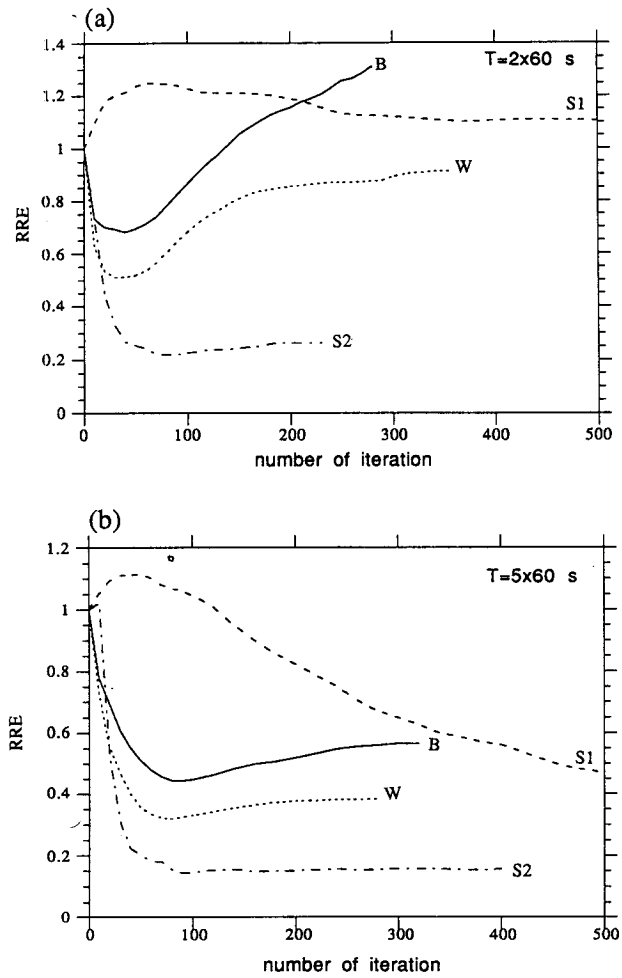

FIG. 3. As in Figs. 2a,b but with error-contaminated data (with 25% relative random temporal fluctuations in the wind field, 25% equation error, and 25% observational error).

the increase of RRE after iteration goes beyond the optimal number, though the cost function J decreases continuously and reaches the minimum at the end of each curve (not shown). To understand this feature, we rewrite the cost function (2.5) as follows:

$$J = \int_0^\tau \int_\Omega \int P(t)(\Delta_1^2 + \Delta_2^2 + 2\Delta_1\Delta_2)\,dydzdt$$

$$\equiv J_1 + J_2 + J_{12},$$

where $\Delta_1 \equiv \eta_e - \eta_t$, $\Delta_2 \equiv \eta_t - \eta_{ob}$, and η_t is the hypothetical reflectivity field advected by the true wind as in (2.4). (If the equation is error-free, then η_t is the true reflectivity field.) If the data and equation are error-free, then $J_2 = J_{12} = 0$ and the RRE should decrease toward the minimum as $J = J_1$ approaches the minimum. However, if the data (or equation) are not error-free, then $J_2 > 0$ and $J_{12} \neq 0$ and, thus, J_1 and the RRE may not decrease toward the minimum as J approaches the minimum. This explains the increase of the RRE beyond the optimal number of iteration along each curve in Figs. 3a,b. For the error-contaminated data, scheme S2 gives the most accurate retrieval. Including more spectral components in (2.16) does not significantly improve scheme S2 but costs more CPU time.

The results of the "optimal" retrievals with the error-contaminated artificial data are shown in Table 2. In this case, scheme S2 gives the best "optimal" retrieval, while scheme W gives the second best "optimal" retrieval. Scheme S1 is most sensitive to errors, as it changes from the best ($N = 5$) in Table 1 to the worst in Table 2. Nevertheless, as shown in Figs. 4a–d, all the retrieved wind fields (for the four schemes with $N = 5$) are quite close to the "true" mean wind field in Fig. 1. But, only scheme S1 and scheme S2 retrieve the wind field that satisfies the mass conservation equation exactly.

c. *Computational efficiency*

The CPU time (on VAX6550) required by each scheme (with $N = 5$) for 100 steps of iteration is listed in the last column of Table 2. As shown, scheme W takes only 3% more CPU time than scheme B. Scheme S2 costs more CPU time than the other three schemes. For the "optimal" retrieval, scheme S1 requires a larger number of iteration, so its costs about the same total CPU time as scheme S2. Scheme W costs much less CPU time than scheme S1 and scheme S2, but the retrieved winds do not accurately satisfy the mass conservation equation (see Table 3). In the next section, we examine how scheme W can be improved and modified into scheme S3, so that the retrieved wind field satisfies the mass conservation equation more accurately.

4. Scheme S3

Scheme S3 is a modified scheme W by applying a postadjustment to the retrieved wind under a strong

TABLE 2. RRE and CPU time for "optimal" retrieval with error-contaminated data.

$\tau = N\Delta\tau$	Scheme	RRE (%)	Number of iterations	CPU time total (s)	CPU time for 100 steps
120 s	B	68.2	40		
	W	51.3	40		
	S1	112.6	280		
	S2	21.9	80		
300 s	B	44.6	80	17.1	21.4
	W	32.0	80	17.6	22.0
	S1	62.9	320	106.8	33.4
	S2	14.6	100	101.5	101.5

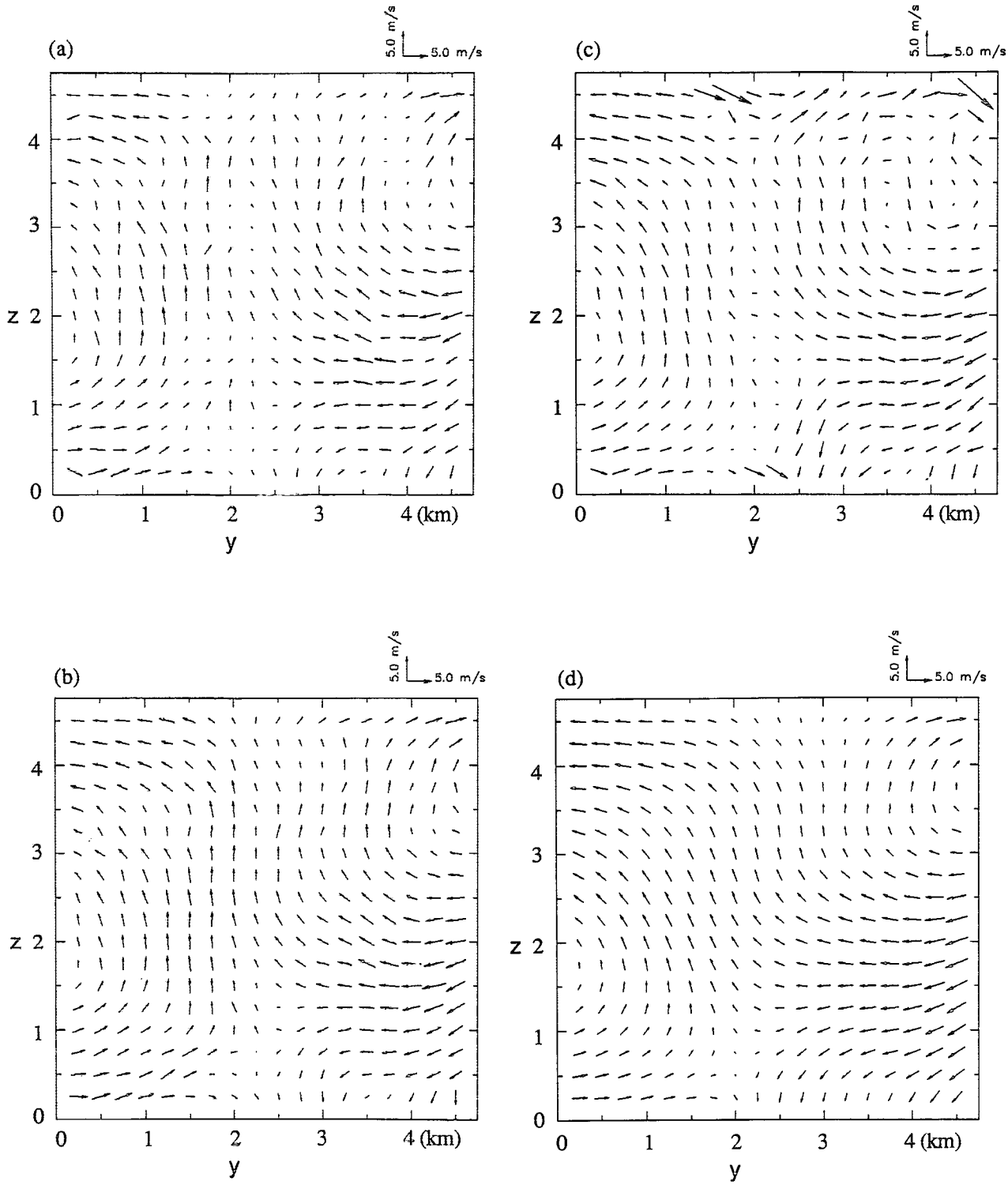

FIG. 4. Retrieved wind fields by (a) scheme B, (b) scheme W, (c) scheme S1, and (d) scheme S2 for experiments with error-contaminated data and $N = 5$ in Table 2.

TABLE 3. Comparison between scheme W and scheme S3 (with error-contaminated data).

$\tau = N\Delta\tau$	Scheme	$\max\lvert\partial_y v_e + \partial_z w_e + \partial_x u_{ob}\rvert$	RRE (%)
120 s	W	1.30×10^{-3} s^{-1}	51.3
	S3	1.36×10^{-5} s^{-1}	50.6
300 s	W	1.38×10^{-3} s^{-1}	32.0
	S3	3.03×10^{-5} s^{-1}	30.1

constraint of mass conservation. Specifically, the postadjustment should minimize the following functional:

$$J_p \equiv \iint_\Omega [a_1(v_e - v_p)^2 + a_2(w_e - w_p)^2]dydz \quad (4.1)$$

under the strong constraint:

$$\partial_y v_p + \partial_z w_p = -\partial_x u_{ob}, \quad (4.2)$$

where (v_e, w_e) is the retrieved wind by scheme W, (v_p, w_p) is the adjusted wind, and a_1 and a_2 are two nondimensional weights. By using the variational method (Sasaki 1970), one can show that the above strongly constrained minimization problem yields $v_p = v_e + (\partial_y\lambda)/2a_1$ and $w_p = w_e + (\partial_z\lambda)/2a_2$, where λ is the Lagrangian multiplier satisfying the following boundary value problem:

$$[(1/2a_1)\partial_y^2 + (1/2a_2)\partial_z^2]\lambda = -(\partial_y v_e + \partial_z w_e + \partial_x u_{ob})$$

within the domain Ω, $\lambda = 0$ at the boundary of Ω. The performances of scheme W and scheme S3 are compared in Table 3, where $a_1 = a_2 = 1$, $k = 500$ s^2, the numbers of iterations used are the same as for scheme W in Table 2, and all the experiments are done with the error-contaminated artificial data (second type). Clearly, the postadjustment is effective. The adjusted wind field satisfies the mass conservation equation much more accurately (though not exactly) than before the postadjustment, and the RRE also becomes slightly smaller.

Since scheme S3 does the adjustment after the fact and accuracy can be lost by dividing the problem into two steps, the final solution is generally further from the wind field implied by the data than the direct retrieval obtained with scheme W. Thus, if the data are error-free and the wind field implied by the data is the "true" field or nearly so, then scheme S3 may not be a good idea, although the solution is adjusted to satisfy the mass conservation equation more accurately. When the data are error contaminated, however, the wind field implied by the data is not the "true" field. As the retrieved wind field is adjusted to satisfy the mass conservation equation more accurately, the solution becomes slightly further from the wind field implied by the data but closer to the "true" wind field. This explains why the RRE is reduced slightly by the postadjustment in scheme S3 as shown in Table 3.

Scheme S3 has nearly the same computational efficiency as scheme W. It was shown in QX92 that scheme B and scheme W can be improved by properly choosing the functional form of weight $P(t)$ in (2.5). Similar improvement can be expected for all other schemes, though $P(t) = 1$ is simply used in this paper. Scheme W and scheme S3 can also be improved by properly choosing the value of weight q [see (2.15) of QX92]. So far, we have chosen $q = k\sigma_\eta^2$ with fixed $k = 500$ s^2. To examine the effect of q on the retrieval, we may still choose $P(t) = 1$ and $q = k\sigma_\eta^2$ but consider

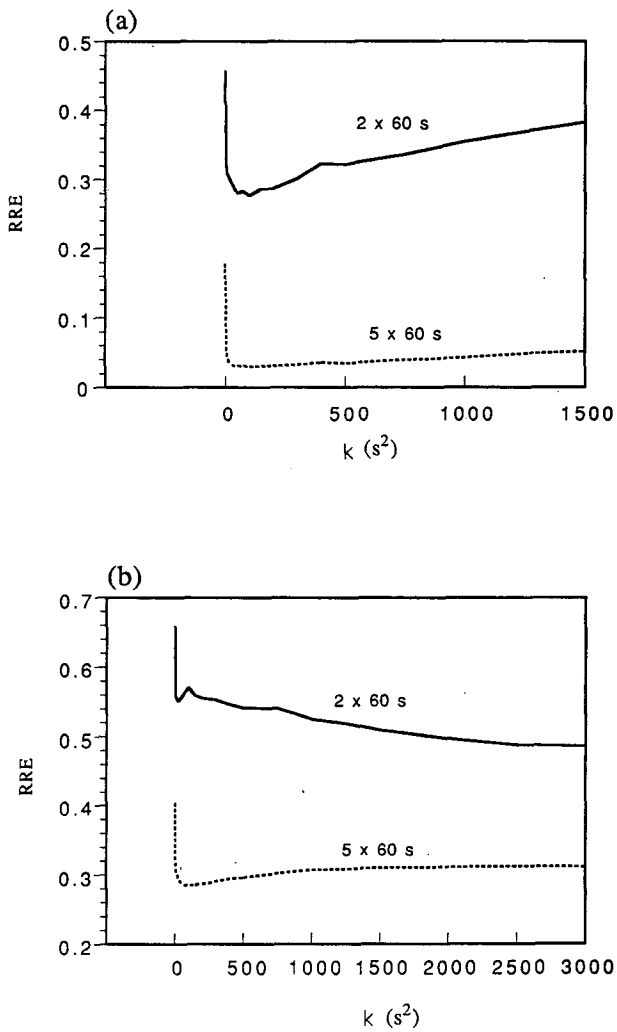

FIG. 5. RRE vs k for experiments with (a) error-free data and (b) error-contaminated data. Here, k is the dimensional coefficient associated with weight q in scheme W. The two curves correspond to $N = 2$ and $N = 5$.

different values for k over a wide range. The results are shown in Figs. 5a,b, where all the experiments are computed by 100 steps of iteration. When the data are error-free (Fig. 5a), $k = 100$ and 50 s^2 give the minimum RREs for $N = 2$ and 5, respectively. For $N = 2$, the RRE increases significantly with k (>100 s^2). For $N = 5$, the RRE remains very small while increasing very slowly with k (>50 s^2). The implication is that the contribution of the mass conservation constraint to the accuracy of the retrieval becomes relatively small when more time levels of observation and, thus, more information are used. When the data are error contaminated (Fig. 5b), the minimum RRE is still around $k = 50$ s^2 for $N = 5$ but shifted to a very large k ($\approx$3000 s^2) for $N = 2$. In general (except for $N = 2$, which is not recommended for our method), k can be chosen over a wide range from 50 to 1000 s^2, while the RRE is close to the minimum and not very sensitive to the value of k.

5. Conclusions

This paper proposes three schemes (S1, S2, and S3) to incorporate a strong mass conservation constraint into the basic scheme of QX92 for retrieving the time-mean winds from a sequence of single-Doppler scans. In scheme S1, the two-dimensional wind field on a surface normal to the radar beam is partitioned into two components: the irrotational component expressed by the velocity potential and nondivergent component expressed by the streamfunction. Since the velocity potential can be obtained directly from the observed radial-component wind divergence (along the radar beam), only the streamfunction needs to be retrieved from the Lagrangian advection of the reflectivity. Scheme S2 is the same as scheme S1 but uses a spectral (instead of grid) representation of the streamfunction and retrieves the spectral coefficients (instead of grid values) of the streamfunction. Tested with artificial data, these two schemes are found to have quite different performances in terms of accuracy, sensitivity to errors, convergence rate, and computational efficiency, though the retrieved wind fields precisely satisfy the mass conservation equation in both schemes. Scheme S1 can be as accurate as scheme W (i.e., the scheme with a weak mass conservation constraint in QX92) only if the data and equation are error-free and the retrieving time is long enough (see Table 1). As shown in Table 2, scheme S2 gives the most accurate retrieval when data are error contaminated (with 25% observational error, 25% equation error, and 25% wind fluctuation). Scheme S2 converges much more rapidly than scheme S1 but takes longer CPU time for each iteration step. Scheme S2 is superior to scheme S1 because it gives the best "optimal" retrieval while costing about the same CPU time as scheme S1. Scheme S3 is a modified scheme W by applying a postadjustment to the retrieved wind under a strong constraint of mass conservation. Tested with the error-contaminated artificial data, scheme S3 is found to be computationally most efficient but less accurate than scheme S2. The retrieved wind field in scheme S3 satisfies the mass conservation equation very accurately, though not precisely (see Table 3).

The relatively slow convergence rate, low computational efficiency, and high sensitivity to data errors for scheme S1 may be explained as follows. First, the cost function (2.5) is directly affected by the estimated velocity rather than streamfunction. As the streamfunction is adjusted along the gradient (2.15) at each grid, the associated velocity adjustment may not be precisely along the gradient of the cost function with respect to the velocity at the same grid. (Note that the latter gradient is not computed in scheme S1.) Second, an adjustment of the streamfunction at one grid changes the velocity at all the adjacent grids, so the adjustments are highly correlated between adjacent grids and cannot give independent contributions to the reduction of the cost function. Since the adjustments are not efficient, the iteration converges slowly. Third, the numerical error is increased when the velocity is computed from the streamfunction through finite differencing.

Similarly, the relatively fast convergence rate, high accuracy, and low sensitivity to data errors for scheme S2 can be understood as follows. First, since the streamfunction and velocity are expressed by the same spectral coefficients, the streamfunction and velocity are adjusted along their respective gradients when the spectral coefficients are adjusted along the gradient of the cost function with respect to the spectral coefficients. Second, the adjustment of each spectral coefficient gives nearly independent contribution to the cost function, so the cost function can be improved effectively. Third, the numerical error does not increase when the velocity is computed directly from the spectral coefficients without using a finite-difference form. These understandings may be useful for developing efficient adjoint methods in general.

Acknowledgments. The authors are thankful to John Lewis, Richard Doviak, and the anonymous reviewers for their comments and suggestions. The financial support for this work was provided by NOAA Contract NA90-RAH00078 and NSF Grants ATM-9113906 at CIMMS and ATM-8809862 at CAPS, University of Oklahoma.

REFERENCES

Batchelor, G. K., 1967: *An Introduction to Fluid Dynamics.* Cambridge University Press, 615 pp.

Cacuci, D. G., 1981: Sensitivity theory for nonlinear system. I: Non-

linear function analysis approach. *J. Math. Phys.*, **22,** 2794–2802.

Haltiner, G. J., and R. T. Williams, 1979: *Numerical Prediction and Dynamic Meteorology.* John Wiley & Sons, 477 pp.

Kapitza, H., 1991: Numerical experiments with the adjoint of a non-hydrostatic mesoscale model. *Mon. Wea. Rev.*, **119,** 2993–3011.

Lynch, P., 1989: Partitioning the wind in a limited domain. *Mon. Wea. Rev.*, **117,** 1492–1500.

Qiu, C. J., and Q. Xu, 1992: A simple adjoint method of wind analysis for single-Doppler data. *J. Atmos. Oceanic Technol.*, **9,** 588–598.

Sasaki, Y. K., 1970: Some basic formalisms in numerical variational analysis. *Mon. Wea. Rev.*, **98,** 875–883.

Talagrand, O., and P. Courtier, 1987: Variational assimilation of meteorological observation with the adjoint vorticity equation. 1: Theory. *Quart. J. Roy. Meteor. Soc.*, **113,** 1311–1328.

Thacker, W. C., and R. B. Long, 1988: Fitting dynamics to data. *J. Geophys. Res.*, **93,** 1227–1240.

Xu, Q., C. J. Qiu, and J. X. Yu, 1994a: Adjoint method retrievals of low-altitude wind fields from single-Doppler reflectivity measured during Phoenix II. *J. Atmos. Oceanic Technol.*, **11,** 275–288.

——, ——, and ——, 1994b: Adjoint method retrievals of low-altitude wind fields from single-Doppler wind data. *J. Atmos. Oceanic Technol.*, **11,** 579–585.